# Rotating polygonal depression soliton clusters on the inner surface of a liquid ring

Hamid Ait Abderrahmane*
*Masdar Institute, Khalifa University of Science and Technology, Masdar City, P.O. Box 54224, Abu Dhabi, United Arab Emirates*

Pooya Soltanian Sedeh, Hoi Dick Ng, and Georgios H. Vatistas
*Department of Mechanical, Industrial and Aerospace Engineering, Concordia University, Montréal, Québec, Canada H3G 1M8*

(Received 13 May 2018; published 14 February 2019)

We report an experimental observation of rotating depression soliton sets on the inner surface of a viscous liquid ring, carrying background waves. These occur within a rotating shallow layer of oil inside a stationary cylindrical container. The solitons are organized either in single, two, or regular polygonal (triangle and hexagon) clusters; they travel in unison at a higher speed than the background traveling waves. The spectral power density reveals a possible energy exchange between the soliton clusters and the background mixed radial-azimuthal modulations through wave radiation.

DOI: 10.1103/PhysRevE.99.023110

## I. INTRODUCTION

Russell in 1834 was the first to observe a soliton (or solitary wave) in the Union Canal in Scotland [1]. This intriguing localized wave pulse was seen to travel along the waterway without appreciable change in its shape and speed. Today this phenomenon is encountered in various physical systems that include water waves [2–8], acoustic waves on a crystal lattice [9], plasmas [10,11], optical fibers [12], conducting polymers [13], superconductors [14], Bose-Einstein condensates [15], DNA dynamics [16], quantum field theory [17], and in the early-Universe cosmology [18]. They are also encountered in technology as in telecommunications [19], optics [20], and information systems processing [21]. Solitons are not limited to very long and shallow media such as channels, fiber optics, electric lines and others, but they also emerge in compact and bounded geometry systems such as liquid droplets [22,23] and confined rotating flows with free surface [24,25].

In 1990, Vatistas reported two phenomena associated with symmetry breaking of free surface in confined rotating flows inside a stationary cylindrical container [26]. The first deals with the formation of rotating polygonal patterns within a water hollow-core vortex, produced by a spinning disk located at the bottom of the tank. The second involves the formation of a revolving solitary wave during drainage of water from a cylindrical container through a small central opening located at the bottom. The former phenomenon has been the focus of sustained research [25,27–33] while the latter has received less attention [24,25].

In this paper, we report the coexistence of both features, associated with the symmetry breaking of free surface in confined rotating flows, namely, the polygonal patterns and revolving circular solitary waves. The phenomenon occurs on the inner surface of a viscous fluid ring, which is formed when a shallow layer of oil is driven in rotation by a revolving circular flat disk inside a stationary cylindrical container. The smooth inner surface of the ring undergoes its first instability that gives rise to azimuthal wave modulations or traveling waves. When these waves are perturbed or the disk speed is increased, they can evolve into regular polygonal or quasipolygonal patterns or stable rotating depression (dark) soliton clusters. These solitons are symmetrically distributed along the interior periphery of the viscous fluid ring; they are organized in groups of single, two, and regular polygonal soliton clusters (triangle and hexagon). It is worth highlighting that the depression soliton is not as common as the single heap type in fluid free-surface dynamics context [2,34,35].

Due to the analogy between the waves in optics and the surface waves in fluids [2], we hypothesize that the observed soliton clusters in the present experiments could be similar to the multisoliton clusters in the form of rotating ringlike found in bulk optical media [36] and to quasipolygonal stable soliton clusters encountered in nonlinear optics [37].

## II. EXPERIMENTAL DETAILS

The experiments were conducted in the apparatus shown schematically in Fig. 1. It consists of a 284-mm-diameter cylindrical container with a sealed bottom and a top open to the atmosphere. A 283-mm-diameter rotating solid disk, firmly attached to an axle, was placed near the bottom. The flywheel shown in the figure dampens any possible fluctuations of the angular velocity of the disk. Since the clearance between the container and the disk was small (1 mm), the evolving phenomenon was assumed to unfold in a stationary vessel with practically a rotating bottom plate. The disk was rotating in the counterclockwise direction, and an electronic controller regulated its speed. The disk imparts angular velocity to a shallow layer of spindle oil (Mobil Velocite Oil No. 6) having a kinematic viscosity of 22.69 cSt. The experiments were conducted at three different fluid heights—8, 10, and 12 mm—of oil above the rotating disk (at rest). The phenomenon was imaged using a CMOS camera (PCO.1200hs

*hamid.abderrahmane@ku.ac.ae

 

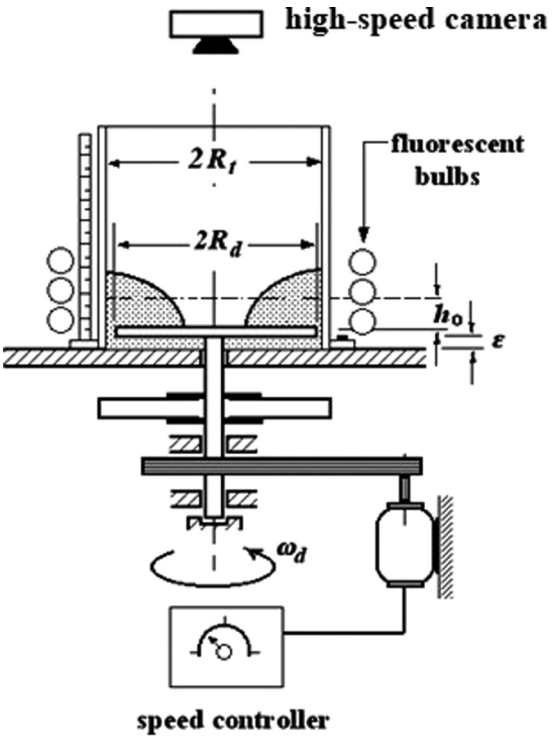


FIG. 1. Schematic of the experimental setup: The present tests were conducted using Spindle Mobil Velocite Oil No. 6. The height of the (quiescent) oil layer $h_0$ was 10 mm, and the disk and tank radii were $R_d = 141$ mm and $R_t = 142$ mm, respectively.

model) mounted on the top of the container to record temporal images of the hollow core. The camera acquired a sequence of resolution of $1280 \times 1024$ pixel images for each mode at a rate of 500 frames per second as 8-bit grayscale. A lighting system consisting of three circular fluorescent bulbs each with 2600 lumens output was used to capture images with the best quality and maximum resolution.

### III. RESULTS AND ANALYSIS

The formation of the oil ring and its inner surface dynamics are first illustrated in Fig. 2. The revolving fluid develops a centrifugal force that pushes the liquid toward the reservoir wall. The retreating liquid exposes part of the surface of the disk to air whereby the line of intersection between the surfaces of the solid disk, the liquid, and air outlines the core shape. For low rotational speeds the oil vortex core remains circular (mode $n = 0$) [see Fig. 2(a)]. At a higher disk speed, the vortex core remains circular but a second circular line appears near the container wall [see Fig. 2(b)]. This line marks a topological change of the fluid region between the wall and the hollow core. The last causes the formation of oil torus or fluid ring, which leans back against the concavity near the wall. By further increasing the disk speed, the inner ring becomes unstable and trains of $n$ waves are propagating around the oil toroid surface as illustrated in Fig. 2(c). By increasing the disk speed much further, the traveling waves evolve into a polygonal pattern (heptagon), as shown in Fig. 2(d).

The instabilities of the oil ring depend on the oil viscosity, the initial oil height, and the disk speed. These give rise to various intriguing dynamics of the inner free surface including, wobbling, breathing, quasistationary, and retrograde modes. However, the most striking of all is the formation of rotating depression solitary wave clusters, shown in Figs. 3 and 4. The soliton clusters are found to travel faster than the traveling waves in the same direction. Besides the single soliton, the rest are symmetrically positioned in the apexes of regular polygons as shown in Figs. 3–5. It is worth highlighting that the soliton clusters are not transient; they persist as long as the disk speed—the control parameter used here—is not varied. While one-soliton and two-soliton states are stable *vis à vis* external perturbations, the triangular and the

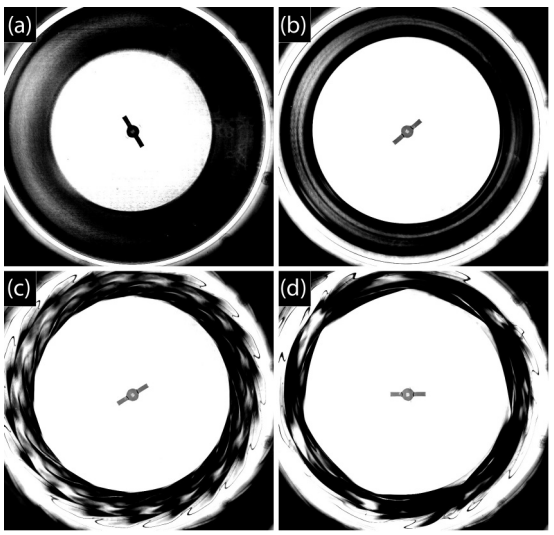


FIG. 2. Formation of the oil ring and the evolution of its inner free surface into a polygonal pattern through traveling waves with increasing disk speed: (a) disk speed = 63 rpm, (b) disk speed = 99 rpm, (c) disk speed = 126 rpm, and (d) disk speed = 155 rpm. Initial oil height $h_0 = 10$ mm.

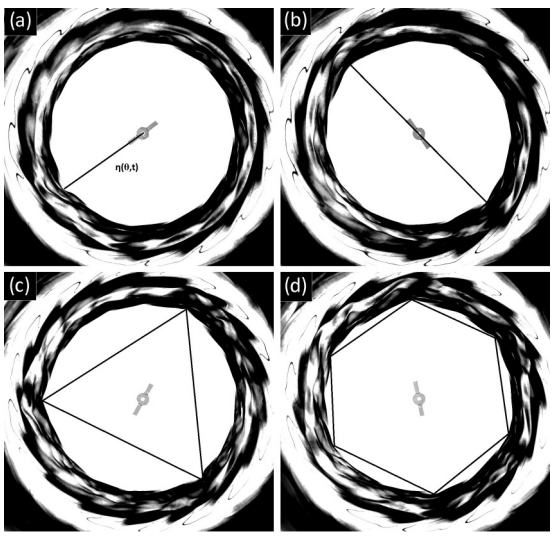


FIG. 3. Cluster of solitary waves observed at $h_0 = 10$ mm: (a) one solitary (disk speed = 114 rpm) wave, (b) two solitary waves (disk speed = 117 rpm), (c) three solitary waves (disk speed = 126 rpm), and (d) six solitary waves (disk speed = 126 rpm).

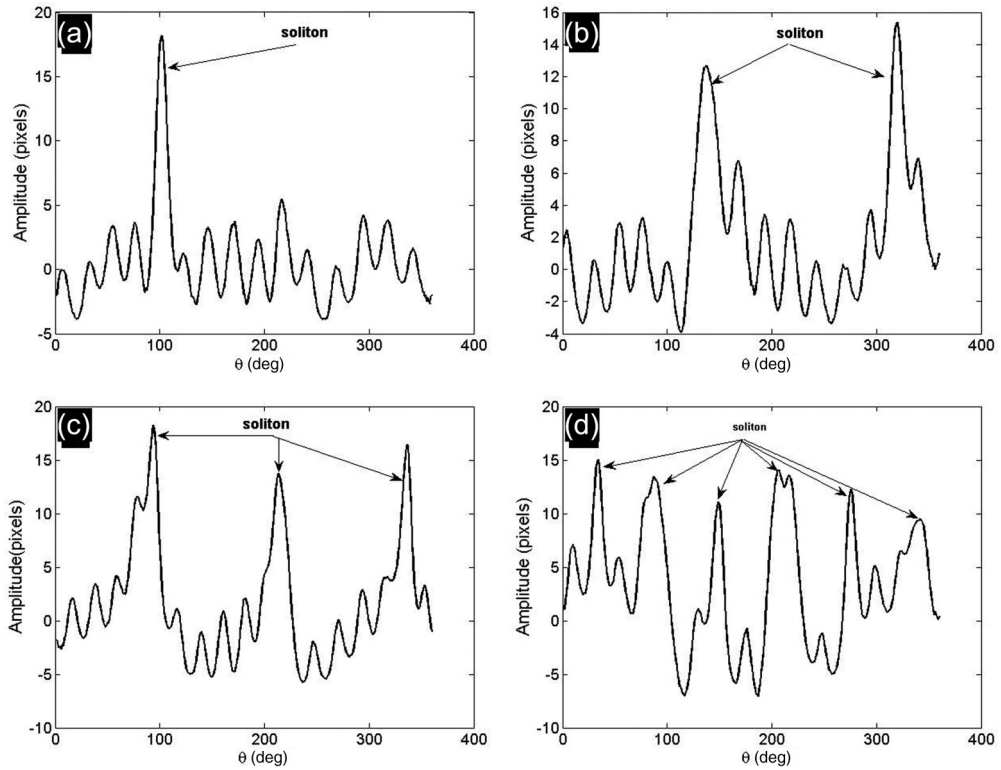


FIG. 4. Solitary wave profiles: (a) one solitary wave, (b) two solitary waves, (c) three solitary waves, and (d) six solitary waves.

hexagonal soliton clusters exchange their stability. In fact, for the same disk speed a perturbation to one of the clusters can cause its bifurcation into another one. Additionally, it is also worth pointing out that clusters of four and five solitons were not observed.

Figure 5 shows the spatiotemporal wave dynamics of the inner surface of the ring, determined using an image processing algorithm implemented in the MATLAB environment. The algorithm includes image segmentation to extract the contours of the inner perimeter of the oil ring shown in Fig. 3. This operation converts the original 8-bit grayscale image into a binary image using a suitable threshold. The noise in the resulting binary image was filtered out using a low-pass Gaussian filter. The contours of the oil ring inner perimeter were extracted using the standard edge detection procedure. These contours were then filtered using a zero-phase filter to ensure that the contours have no phase distortion.

In Fig. 5, the white lines correspond to the waves of highest amplitudes (solitons), stemming from the angle axes ($t = 0$ s). Figure 5 shows a set(s) of one, two, three, and six solitons traveling in unison around the inner surface of the fluid ring. The soliton clusters coexist with large wave number background traveling waves. These waves have relatively smaller amplitudes in comparison to those of the solitons. Video recordings, showing the orbiting soliton clusters and traveling waves on the inner surface of the oil ring, are provided in the Supplemental Material [38].

To deepen our understanding of the wave dynamics on the inner perimeter of the oil ring, the spectral energy density method was used to predict the dispersion relations. The full space and time-resolved power spectrum of wave amplitude, $S_\eta(\omega, k)$, was computed from each set of inner perimeter contour deformation $\eta(\theta, t)$. We performed successively Fourier transforms in both space and time on $\eta(\theta, t)$, depicted in Fig. 6. The operation was performed on 4000 images, taken at 500 frames per second, corresponding to a duration of approximately 8 s. The spatiotemporal power spectra $S_\eta(\omega, k)$ of the free-surface displacement $\eta(x, t)$ as a function of the dimensionless wave number $k$ and the angular frequency $\omega$ are shown in Fig. 6. This figure represents the experimental dispersion relations, corresponding to the distribution of energy over the Fourier space ($\omega \equiv 2\pi f, k \equiv 2\pi/\lambda$) where $\lambda$ is the dimensionless wavelength and $f$ is the frequency of the waves. Equivalently, Fig. 7 gives the spatial amplitude for all time signals analyzed.

From Fig. 6 it is shown that the energy of the wave dynamics is distributed over relatively large intervals of angular frequency $\omega$ and dimensionless wave number, $k$. Angular frequency $\omega$ ranges from 0 to 30 rad/s, while $k$ spans from 0 to approximately 2.8. The resulting wave spectra or the experimental dispersion relations depicted in Figs. 6(a)–6(d) consist mainly of three branches (outlined by the dashed lines). The large numbers of discrete peaks, corresponding to relatively high wave amplitudes, are clustered along the main branch (straight lines in Fig. 6). This stands for the rotating solitons, their amplitude modulations, and the wave dynamics in their vicinity, which are triggered as they travel and interact with the background waves (see Figs. 4 and 7). This can explain the fact that the wave spectrum or the Fourier transform is spread over large intervals $(\omega, k)$ along the main branch. It is worth recalling that the wavelength $\lambda$ is defined as $2\pi/n$ where $n$ is an integer which represents the wave mode or the number of crests along the perimeter. In other words, the wave number $k$ is defined as $n/2\pi$.

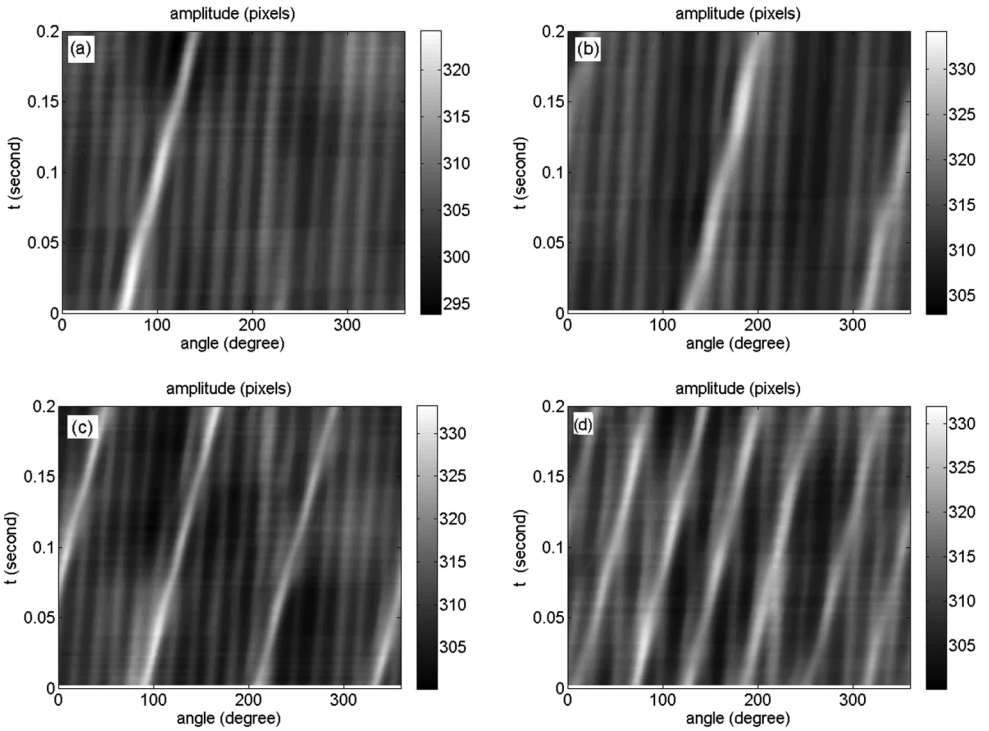


FIG. 5. Unwound surface contours depicted in the space-time $(\theta, t)$ plane. Soliton clusters (brighter) on background traveling waves: (a) one solitary wave, (b) two solitary waves, (c) three solitary waves, and (d) six solitary waves.

The second branch locates above the main one, and reveals the existence of a frequency cutoff and an asymptotic wave number. From Fig. 6(a) the cutoff angular frequency and the wave number are approximately $\omega_c = 7\,\mathrm{rad/s}$ and $k_c = 0.65$, respectively. The asymptotic dimensionless wave number corresponds to the mode $n \approx 4\,(n = 0.65 \times 2\pi)$.

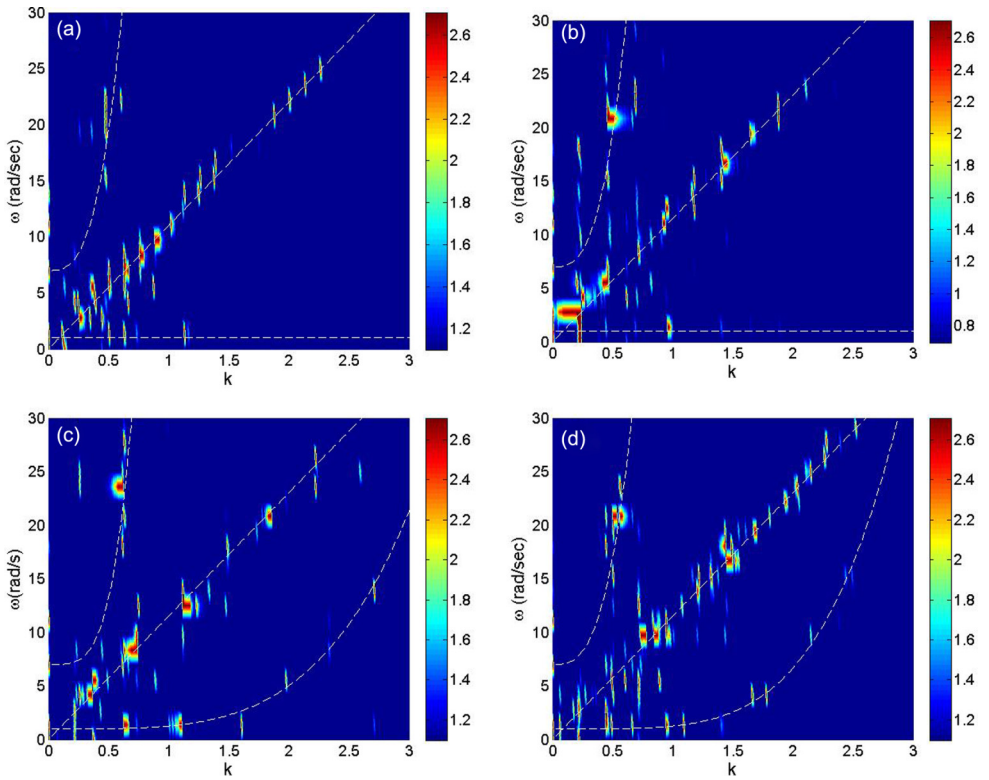


FIG. 6. Power spectra $S_\eta(k, \omega)$ of the inner interface of the fluid ring, $\eta(x, t)$: (a) one solitary wave, (b) two solitary waves, (c) three solitary waves, and (d) six solitary waves.

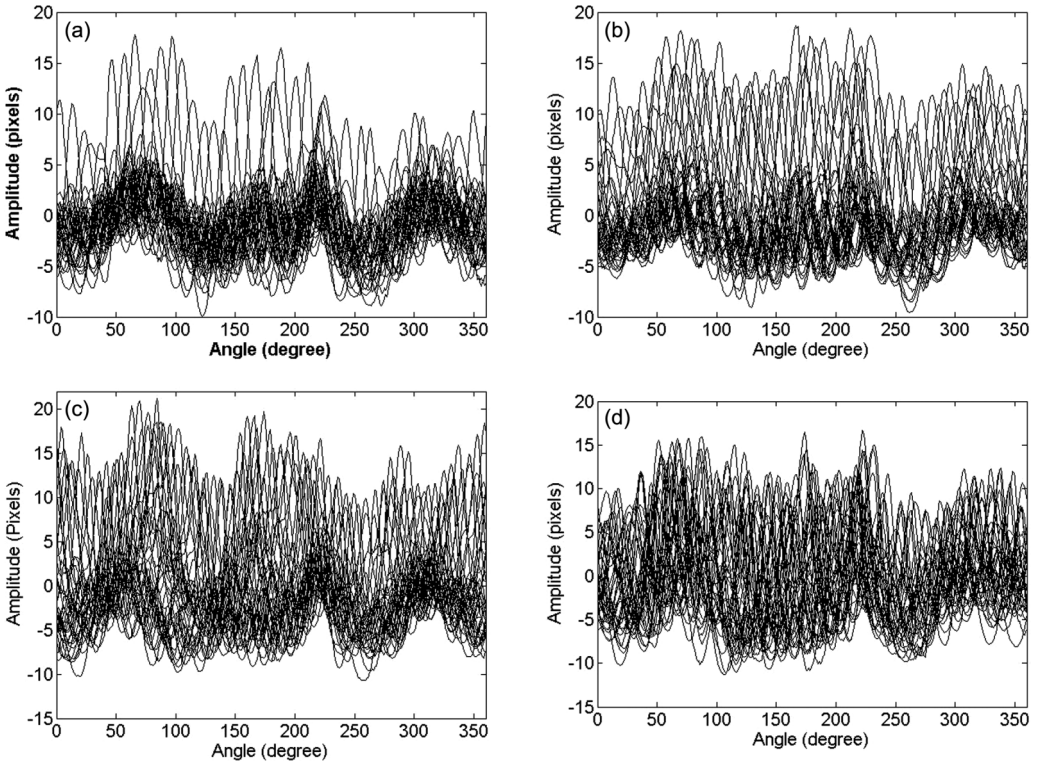


FIG. 7. Spatiotemporal wave dynamics of the inner surface of the ring: (a) one solitary wave, (b) two solitary waves, (c) three solitary waves, and (d) six solitary waves.

The second branch stands for the radial modulation of the ring shape, which appears as a quasistanding wave of wave number $n = 4$ in Fig. 7(a). This quasistanding wave or the radial modulation of the oil ring inner perimeter, should correspond to a kind of breathing or varicose mode of the oil ring. Similar quasistanding waves with wave number $n = 4$ are found in Figs. 6(b)–6(d) and Figs. 7(b) and 7(c). Although captured in Fig. 6(d), the quasistanding wave with $n = 4$ is not as clear in Fig. 7(d), possibly due to their strong interaction with the hexagonal soliton cluster and the traveling waves. The latter propagate at constant speeds but slower than the soliton cluster; they are depicted in Fig. 6 by the third branch, which lies below the main one.

The third branch of the dispersion curves shows that the energy of the traveling waves is distributed over a large scale of dimensionless wave numbers $k$. For instance, the horizontal straight lines in Figs. 6(a) and 6(b) spread over a large dimensionless wave number interval that extends up to approximately $k = 2.4$, which corresponds to $n = 15$ ($n = 2.4 \times 2\pi$). This is consistent with the number of traveling waves depicted in Figs. 5(a) and 5(b). In Figs. 6(c) and 6(d), the third branch becomes convex but remains below the main one, which means that the speed of the traveling waves remains slower than that of the soliton clusters. The upper limit of the dimensionless wave number, $k$, increases slightly, which corresponds to a higher mode of traveling waves, i.e., $n = 17$ and $n = 16$, respectively [see Figs. 5(c) and 5(d)]. However, a traveling wave with $n = 16$ is barely visible in Fig. 5(d). As indicated previously, this is possibly due to the strong interactions between the three types of waves depicted by the three dispersion relation branches above.

In Fig. 6, one can also notice the energy distribution over discrete wave number and angular frequency intervals between the three branches or dispersion curves. Since the oil ring can be considered as a compact bounded geometry or as a closed system in itself, the presence of discrete points, $(k, \omega)$, between branches suggests energy exchange, through wave radiation between the mixed radial-azimuthal modulations (background waves) and the soliton clusters. This may also explain the shift of the third branch toward the higher frequencies and its convexity in Figs. 6(c) and 6(d). The convexity of the third branch can be also interpreted as a rise of wave dispersion.

The present research shows that a rotating shallow layer of spindle oil can lead to the formation of a fluid ring. The initial ring with a smooth and circular inner surface develops a first instability. This leads eventually to the formation of quasistationary and traveling background waves. We found in this work that the fluid ring carrying mixed radial-azimuthal modulations can evolve into single, two, triangular, and hexagonal soliton clusters. Here, we test whether or not the well-known Korteweg–de Vries theoretical $\text{sech}^2$ profile curve fits the experimental profile of the soliton in space and time (see Fig. 8). It shows that the profile of the soliton in space can be curve fitted fairly well in *space* by $\text{sech}^2$. However, considering the soliton celerity, the $\text{sech}^2$ profile does not match well the profile in *time*. This may perhaps suggest that the observed clusters of depression solitary waves cannot be fully modeled by the Korteweg–de Vries equation. Consequently, one should explore the possibility whether they can be described by other well-known nonlinear equations such as the nonlinear Schrödinger or cubic-quintic complex

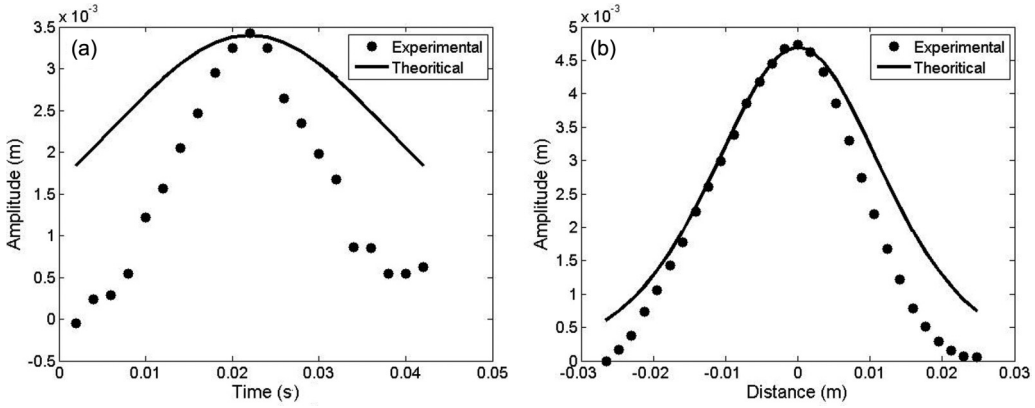


FIG. 8. Curve fitting of the typical experimental soliton by $\mathrm{sech}^2$ profiles: (a) in time and (b) in space.

Ginzburg-Landau equation, which describe fundamental soliton and polygonal soliton clusters [37,39].

## IV. CONCLUDING REMARKS

The polygonal soliton clusters reported in this contribution give rise to a new paradigm. Although these soliton clusters were observed in the same apparatus that we have used in the past, they are fundamentally different from those found in a shallow layer of water. In fact, the polygonal patterns observed in a shallow layer of water occur in the inner solid-body region of the hollow core vortex, while the polygonal soliton clusters reported here occur in a thin spindle oil ring. The oil ring topology is most probably due to the shear thinning propriety of spindle oil and not only to the oil viscosity. In fact, the pattern observed with various glycerin-water mixtures, much more viscous than water, resembles the one observed with water [29]. The observed solitons appear to be of nearly the same amplitude and they occur in a very narrow range of the rotating disk speed (between 114 and 126 rpm). The control of the conditions of their occurrence remains elusive; their occurrence depends on various parameters, e.g., type of oil, disk speed, initial height of the oil, and perhaps surface tension.

Various explanations of the polygonal patterns in water can be found in the literature depending on the model of the hollow-core vortex. For instance, the patterns are explained as a resonance between gravity and centrifugal waves, when the hollow-core vortex is considered as potential [40]. When the hollow-core vortex is modeled as a Rankine vortex, the polygonal patterns are explained as the result of the interaction between gravity and "Kelvin-centrifugal" waves [41]. Contrasting with the wave approach of the polygonal patterns phenomenon, these are seen as Kelvin's equilibria or a result of the satellite vortices at the apexes of the polygonal patterns [26–28]. Unlike water used in the aforementioned studies on the formation of polygonal patterns, the non-Newtonian properties of the Spindle oil possibly give rise to the dynamical behavior observed in this work.

It is worth noting that the polygonal soliton clusters observed here on an oil ring, which can be considered as compact bounded geometry, can be related to those unfolding in another compact bounded geometry, namely, liquid drop. In fact, the present liquid ring can be considered as topologically similar to liquid drop. The latter is known to support traveling wave solutions, which can evolve from small oscillations to cnoidal waves, and to solitary waves [22,42]. It is worth noting that liquid drop paradigm was used to give reason to a diverse set of scientific and technological problems [23].

[1] J. S. Russell, Proc. R. Soc. Edinburgh **11**, 319 (1844).
[2] A. Chabchoub, O. Kimmoun, H. Branger, N. Hoffmann, D. Proment, M. Onorato, and N. Akhmediev, Phys. Rev. Lett. **110**, 124101 (2013).
[3] R. Grimshaw, *Solitary Waves in Fluids* (WIT Press, Southampton, UK, 2007).
[4] W. K. Melville, G. G. Tomasson, and D. P. Renouard, J. Fluid Mech. **206**, 1 (1989).
[5] C. Katsis and T. Akylas, Phys. Fluids **30**, 297 (1987).
[6] R. Grimshaw, Stud. Appl. Math. **73**, 1 (1985).
[7] W. G. Pritchard, J. Fluid Mech. **42**, 61 (1970).
[8] T. B. Benjamin, J. Fluid Mech. **29**, 559 (1967).
[9] H.-Y. Hao and H. J. Maris, Phys. Rev. B **64**, 064302 (2001).
[10] J. L. Shohet, Eur. Phys. J. Spec. Top. **147**, 191 (2007).
[11] N. J. Zabusky and M. D. Kruskal, Phys. Rev. Lett. **15**, 240 (1965).
[12] L. F. Mollenauer, R. H. Stolen, and J. P. Gordon, Phys. Rev. Lett. **45**, 1095 (1980).
[13] W. P. Su, J. R. Schrieffer, and A. J. Heeger, Phys. Rev. Lett. **42**, 1698 (1979).
[14] Y. Tanaka, Phys. Rev. Lett. **88**, 017002 (2001).
[15] A. Weller, J. P. Ronzheimer, C. Gross, J. Esteve, M. K. Oberthaler, D. J. Frantzeskakis, G. Theocharis, and P. G. Kevrekidis, Phys. Rev. Lett. **101**, 130401 (2008).
[16] M. Vanitha and M. Daniel, Phys. Rev. E **85**, 041911 (2012).
[17] V. Schön and M. Thies, Phys. Rev. D **62**, 096002 (2000).
[18] J. A. Frieman, G. B. Gelmini, M. Gleiser, and E. W. Kolb, Phys. Rev. Lett. **60**, 2101 (1988).
[19] V. E. Zakharov and S. Wabnitz, *Optical Solitons: Theoretical Challenges and Industrial Perspectives* (Springer-Verlag, Berlin, 1999).

[20] M. Peyrard and T. Dauxois, *Physics of Solitons* (Cambridge University Press, Cambridge, England, 2006).
[21] H. A. Haus and W. S. Wong, Rev. Mod. Phys. **68**, 423 (1996).
[22] A. Ludu, *Boundaries of a Complex World* (Springer, New York, 2016).
[23] A. Ludu and J. P. Draayer, Phys. Rev. Lett. **80**, 2125 (1998).
[24] M. Amaouche, H. A. Abderrahmane, and G. H. Vatistas, Phys. Rev. E **87**, 043015 (2013).
[25] H. A. Abderrahmane, M. Amaouche, M. Fayed, H. D. Ng, G. H. Vatistas, and K. Siddiqui, Phys. Rev. E **84**, 037302 (2011).
[26] G. H. Vatistas, J. Fluid Mech. **217**, 241 (1990).
[27] H. A. Abderrahmane, M. Fayed, H. D. Ng, and G. H. Vatistas, J. Fluid Mech. **724**, 695 (2013).
[28] G. H. Vatistas, H. A. Abderrahmane, and M. H. Kamran Siddiqui, Phys. Rev. Lett. **100**, 174503 (2008).
[29] H. A. Abderrahmane, M. Fayed, H. D. Ng, and G. H. Vatistas, Exp. Therm. Fluid. Sci. **87**, 104 (2017).
[30] H. A. Abderrahmane, K. Siddiqui, and G. H. Vatistas, Exp. Fluids **50**, 677 (2011).
[31] T. R. N. Jansson, M. P. Haspang, K. H. Jensen, P. Hersen, and T. Bohr, Phys. Rev. Lett. **96**, 174502 (2006).
[32] K. Iga, Fluid Dyn. Res. **49**, 065502 (2017).
[33] B. Bach, E. Linnartz, M. Vested, A. Andersen, and T. Bohr, J. Fluid Mech. **759**, 386 (2014).
[34] E. Falcon, C. Laroche, and S. Fauve, Phys. Rev. Lett. **89**, 204501 (2002).
[35] D. Rannacher and A. Engel, New J. Phys. **8**, 108 (2006).
[36] A. S. Desyatnikov and Y. S. Kivshar, Phys. Rev. Lett. **88**, 053901 (2002).
[37] Y. He, D. Mihalache, B. A. Malomed, Y. Qiu, Z. Chen, and Y. Li, Phys. Rev. E **85**, 066206 (2012).
[38] See Supplemental Material at http://link.aps.org/supplemental/10.1103/PhysRevE.99.023110 for a movie showing a cluster of deep solitary waves traveling around a polygonal torus pattern.
[39] Z. Yuan, J. Wang, M. Chu, G. Xia, and Z. Zheng, Phys. Rev. E **88**, 042901 (2013).
[40] L. Tophøj, J. Mougel, T. Bohr, and D. Fabre, Phys. Rev. Lett. **110**, 194502 (2013).
[41] J. Mougel, D. Fabre, and L. Lacaze, Mech. Ind. **15**, 107 (2014).
[42] A. Ludu, *Nonlinear Waves and Solitons on Contours and Closed Surfaces* (Springer, New York, 2012).